APPLIED SCIENCES AND ENGINEERING

Nanotransfection-based vasculogenic cell reprogramming drives functional recovery in a mouse model of ischemic stroke

Luke R. Lemmerman[1], Maria H. H. Balch[2], Jordan T. Moore[1], Diego Alzate-Correa[1], Maria A. Rincon-Benavides[1], Ana Salazar-Puerta[1], Surya Gnyawali[2], Hallie N. Harris[2], William Lawrence[1,3], Lilibeth Ortega-Pineda[1], Lauren Wilch[4], Ian B. Risser[1], Aidan J. Maxwell[5], Silvia Duarte-Sanmiguel[1,6], Daniel Dodd[1,3], Gina P. Guio-Vega[1,7], Dana M. McTigue[8], W. David Arnold[9], Shahid M. Nimjee[2], Chandan K. Sen[10], Savita Khanna[10], Cameron Rink[2], Natalia Higuita-Castro[1,11]*, Daniel Gallego-Perez[1,11]*

Ischemic stroke causes vascular and neuronal tissue deficiencies that could lead to substantial functional impairment and/or death. Although progenitor-based vasculogenic cell therapies have shown promise as a potential rescue strategy following ischemic stroke, current approaches face major hurdles. Here, we used fibroblasts nanotransfected with *Etv2*, *Foxc2*, and *Fli1* (*EFF*) to drive reprogramming-based vasculogenesis, intracranially, as a potential therapy for ischemic stroke. Perfusion analyses suggest that intracranial delivery of *EFF*-nanotransfected fibroblasts led to a dose-dependent increase in perfusion 14 days after injection. MRI and behavioral tests revealed ~70% infarct resolution and up to ~90% motor recovery for mice treated with *EFF*-nanotransfected fibroblasts. Immunohistological analysis confirmed increases in vascularity and neuronal cellularity, as well as reduced glial scar formation in response to treatment with *EFF*-nanotransfected fibroblasts. Together, our results suggest that vasculogenic cell therapies based on nanotransfection-driven (i.e., nonviral) cellular reprogramming represent a promising strategy for the treatment of ischemic stroke.

INTRODUCTION

Stroke is the second leading cause of death worldwide and the third leading cause of morbidity (*1*). The disabilities patients suffer from stroke include paralysis, sensory impairment including vision and speech impairment, and death (*2*). In the United States, a stroke occurs every 40 s, with a death rate of ~20% and a financial burden that is expected to reach ~$100 billion by 2035 (*2*). Risk factors of stroke include tobacco abuse, sedentary lifestyle, diabetes mellitus, hypertension, and hyperlipidemia (*2*). Currently, recombinant tissue plasminogen activator (rtPA) and endovascular thrombectomy (EVT) are the only U.S. Food and Drug Administration–approved interventions for acute treatment of ischemic stroke (*3*, *4*). However, rtPA and EVT implementation is restricted to the first 3 to 4.5 hours and 24 hours after last known well, respectively, limiting their use to less than 20% of patients (*3*, *5*). Moreover, these treatments solely focus on recanalizing the occluded blood vessel and do not aid the repair of damaged tissue (*6*). Hence, there is still a need for effective therapies to attenuate tissue damage and aid repair after stroke. Recent studies show that therapies solely aimed at boosting endogenous tissue repair via pharmacologic/trophic factors are often inefficient (*7*–*9*). Alternative approaches are thus still needed.

Cell-based therapies have emerged as a promising alternative strategy for the resolution of structural and/or functional cellular deficits after stroke (*6*, *9*). Progenitor-based vascular cell therapies, in particular, implemented within days after stroke, have been shown to lead to improved neurological recovery by leveraging the synergy that exists between neurogenic and vasculogenic processes during nerve tissue repair and/or development (*10*). However, current approaches to vascular cell therapies for stroke still face major hurdles, as they tend to rely on progenitor cell populations that are scarce and/or functionally impaired, especially in patients with comorbidities such as diabetes (*11*, *12*). Moreover, progenitor-based cell therapies carry additional risks in terms of uncontrolled differentiation, tumorigenesis, genetic abnormalities, and immunogenicity (*6*, *13*).

Recent advances in direct cell reprogramming have opened up the possibility for developing patient-specific cell therapies that circumvent many of the above-mentioned limitations, by using more abundant and readily available cell sources (e.g., skin fibroblasts) (*14*), and bypassing the need for induced pluripotency and the risks associated with it (*15*). However, current approaches to direct cell reprogramming still face multiple barriers including biosafety concerns associated with viral transfections, as well as capsid size constraints on reprogramming cargo (*16*). Various chemical and physical transfection methods have thus been developed in light of these concerns. Nevertheless, chemical methods (e.g., lipo/polyplex-based nanocarriers) rely heavily on endocytosis to achieve transfection, and thus, endosomal escape poses a major challenge. While physical methods such as biolistic transfection (e.g., gene gun) can be

[1]Department of Biomedical Engineering, The Ohio State University, Columbus, OH 43210, USA. [2]Department of Neurosurgery, The Ohio State University, Columbus, OH 43210, USA. [3]Biomedical Sciences Graduate Program, The Ohio State University, Columbus, OH 43210, USA. [4]Coulter Department of Biomedical Engineering, Georgia Institute of Technology, Atlanta, GA 30332, USA. [5]Department of Biology, The Ohio State University, Columbus, OH 43210, USA. [6]OSU Nutrition, The Ohio State University, Columbus, OH 43210, USA. [7]Department of Medicine, National University of Colombia, Bogotá, Colombia [8]Department of Neuroscience, The Ohio State University, Columbus, OH 43210, USA. [9]Department of Neurology, The Ohio State University, Columbus, OH 43210, USA. [10]Department of Surgery, Indiana University School of Medicine, Indianapolis, IN 46202, USA. [11]Department of Surgery, The Ohio State University, Columbus, OH 43210, USA.
*Corresponding author. Email: gallegoperez.1@osu.edu (D.G.-P.); higuitacastro.1@osu.edu (N.H.-C.)

applied to a host of cells, these could cause substantial cell damage, and the gold/tungsten carriers may also have a negative impact on cell functionality. Bulk electroporation (BEP), on the other hand, is a simple and rapid transfection method that has been widely used in both basic research and translational applications. BEP-based transfection, however, is still partially driven by endocytosis and endosomal escape (*17*), with the electric field mainly facilitating binding of the genetic cargo to the cell surface to then be internalized through an endocytosis-like process. Moreover, the high-magnitude and nonuniform voltage used during BEP also results in low cell viability in most cases (*18*, *19*).

Recently, we reported on a simple-to-implement, nanotransfection-based approach to nonviral cell and tissue reprogramming (*18*, *19*). We found that nanochannel-driven delivery of a cocktail containing the developmental transcription factor genes *Etv2*, *Foxc2*, and *Fli1* (*EFF*) can drive de novo formation of induced endothelial cells (iECs) and new vascular tissue via reprogramming of stromal tissue (e.g., fibroblasts), which effectively countered tissue degeneration in a mouse model of limb ischemia. Here, we report on the use of nanotransfection-based direct vasculogenic reprogramming approaches for the treatment of cerebral ischemia. Our results indicate that intracranial delivery of fibroblasts nanotransfected with the *EFF* cocktail leads to dose-dependent increases in perfusion, reduced stroke volume, and significant recovery of locomotive abilities in stroke-affected mice.

RESULTS AND DISCUSSION

Intracranial delivery of *EFF*-nanotransfected fibroblasts is associated with increased intracranial perfusion in healthy mice

Transwell inserts were adapted into nanotransfection platforms as reported previously (*18*, *19*), with few modifications, and were used to transfect primary mouse embryonic fibroblasts (pMEFs) with a cocktail of plasmids encoding for *EFF* at a 1:1:1 ratio. Briefly, pMEFs grown to confluency on the apical portion of a transwell insert were sandwiched between Au-plated electrodes using a custom-made electrotransfection setup. The basal portion of the transwell rested on a polydimethylsiloxane reservoir containing the plasmid solution. A pulsed electric field (~27.5 V/mm, 35-ms pulses, 10 pulses) was then applied across the electrodes to nanoporate the cell membranes and electrophoretically drive the plasmids into the cells (Fig. 1A). Nanotransfection of pMEFs with sham/empty plasmids (i.e., pCMV6) served as control. Quantitative reverse transcription polymerase chain reaction (qRT-PCR) analyses at days 1 and 7 after nanotransfection showed a robust increase of *EFF* expression as compared to controls (Fig. 1B and fig. S1). Immunofluorescence and tube formation assays at day 7 confirmed the ability of *EFF*-nanotransfected pMEFs to exhibit phenotypic changes consistent with fibroblast-to-iEC transitions (Fig. 1D) and to assemble into blood vessel–like vascular networks in vitro (Fig. 1E). These findings were in accordance with our previous study, where we reported iEC-directed conversion rates of approximately 17% and tube formation ability by day 7 (*19*). qRT-PCR analyses showed that *EFF* nanotransfection also led to an increase in proangiogenic (i.e., *bFGF*) and prolymphogenic (i.e., *VEGF-D*) gene expression in pMEF cultures as early as day 1 (Fig. 1B and fig. S1). Moreover, analysis of exosomal components (fig. S2, A and B) in the supernatant indicated that *EFF* transcripts were also prevalent in pMEF-derived exosomes following *EFF* nanotransfection, with proangiogenic transcripts such as *bFGF* also trending upward ($P = 0.08$) (Fig. 1C). No significant changes, however, were observed in proangiogenic/lymphogenic factor expression or exosomal loading, at the protein level, at day 1 after nanotransfection (figs. S1 and S2). Notably, intracranial injection of pMEFs into the subarachnoid space (fig. S3) of 9-week-old C57BL/6 mice, 24 hours after *EFF* nanotransfection, led to a marked increase in intracranial perfusion 7 days after cell delivery compared to controls (Fig. 1, F and G), as confirmed by laser speckle imaging (LSI), thus suggesting that *EFF*-nanotransfected fibroblasts could potentially be used to address ischemic disorders in brain tissue.

While we previously reported that *EFF*-nanotransfected skin tissue (in vivo) can also produce exosomes laden with *EFF* and proangiogenic transcripts that could independently initiate provasculogenic/angiogenic responses in vitro and in vivo (*19*), the heterogeneity of skin tissue made it difficult to determine the extent to which such exosomal transcripts were emanating from preexisting vascular versus nonvascular cells in the skin. In this study, however, we showed that purified fibroblast populations nanotransfected with *EFF*, in vitro, also have a tendency to produce exosomes loaded with provasculogenic/angiogenic transcripts. The implications of these observations are twofold, as it suggests that increased intracranial perfusion could potentially be modulated, in part, by a combination of (i) iEC-directed reprogramming of a proportion of the injected pMEFs, some of which appear to cross over to the contralateral hemisphere, and (ii) exosome-driven autocrine and/or paracrine vasculogenesis or angiogenesis from preexisting vascular tissue (*20*).

Stroke-affected mice treated with *EFF*-nanotransfected fibroblasts show increased vascularization and intracranial perfusion

Once we established the ability of *EFF*-nanotransfected pMEFs to increase the perfusion level of healthy brain tissue, we proceeded to test whether *EFF*-nanotransfected pMEFs can also increase the perfusion levels of stroke-affected brains (Fig. 2). For this, we induced 30-min ischemic strokes in the right hemisphere of 9-week-old C57BL/6 mice using the middle cerebral artery occlusion (MCAO) method (Fig. 2A). *EFF*- or sham-nanotransfected pMEFs were injected intracranially (i.e., 24 hours after nanotransfection) into the subarachnoid space above the stroke-affected sensorimotor cortex on day 7 after stroke toward the end of the acute/inflammatory stage (Fig. 2A) (*21*, *22*). Next, mice were monitored for 21 days after stroke, and LSI was used to evaluate cerebral perfusion through the intact skull. LSI analyses revealed a positive correlation between the number of *EFF*-nanotransfected cells and the perfusion levels for both the stroke-affected (ipsilateral) hemisphere and contralateral hemisphere (Fig. 2, B and C). No correlation was found between perfusion and the number of sham-nanotransfected cells. Immunostaining for standard endothelial cell markers, CD31 and *Ricinus communis* agglutinin I (RCA) lectin (*23*), identified significantly higher immunoreactivity in the ipsilateral and contralateral hemisphere of *EFF*-treated mice, suggesting increased vascularity compared to sham controls (Fig. 2, D and E). Bilateral effects were possibly due, in part, to intracranial spread of *EFF*-nanotransfected pMEFs (figs. S3 and S4) and/or provasculogenic *EFF*-laden exosomes (*19*, *24*, *25*). While cell spreading to the contralateral hemisphere did not seem to have any detrimental effect in this study, for more localized cell therapeutics, additional injection/deployment approaches may be needed.

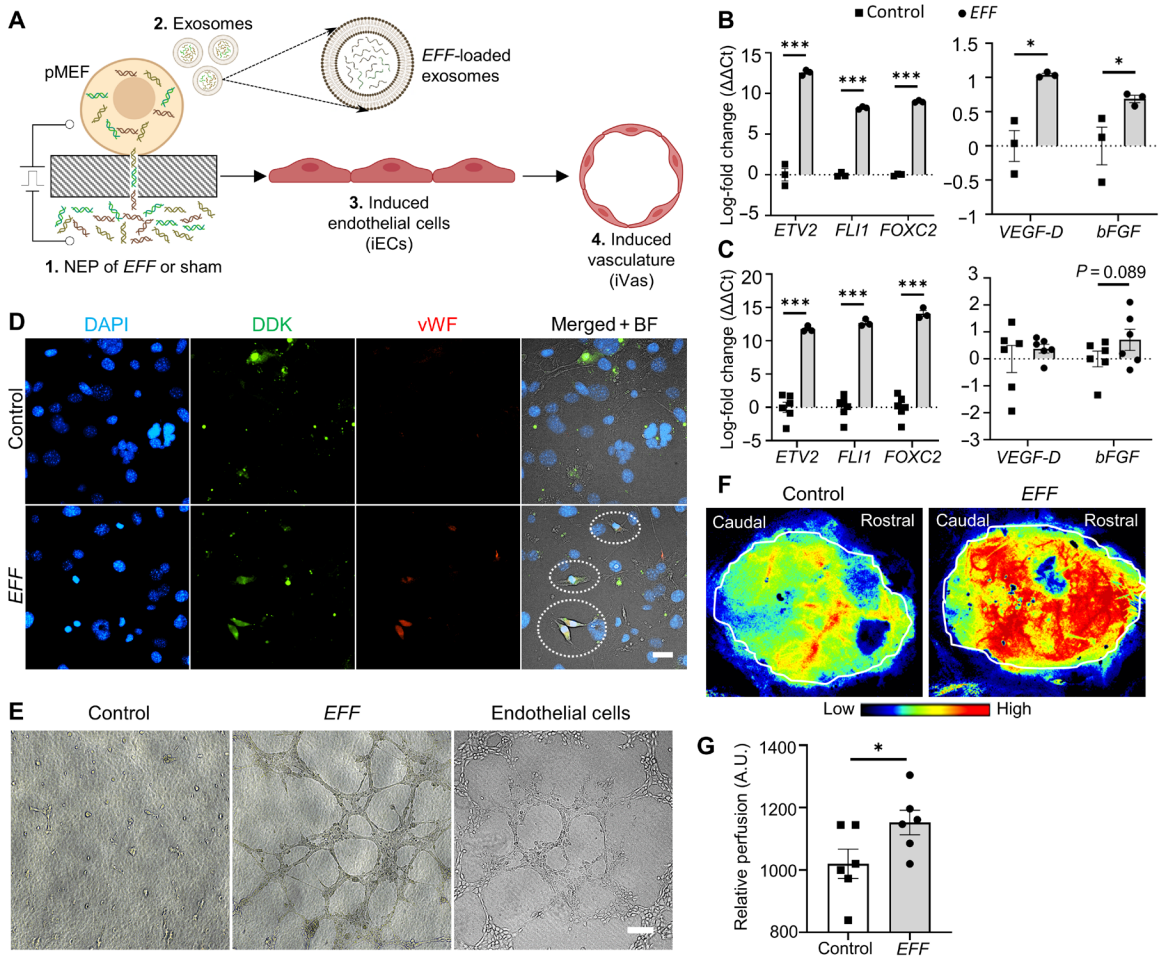

Fig. 1. *EFF*-nanotransfected fibroblasts demonstrate successful vasculogenic reprogramming and drive increased perfusion in healthy brain tissue. (**A**) Schematic diagram illustrating the procedure for pMEF nanotransfection and subsequent biological changes, including the release of provasculogenic/angiogenic exosomes, and nuclear reprogramming conducive to the derivation of induced endothelial cells (iECs) and de novo formation of induced vasculature (iVas). (**B**) *EFF*, *VEGF-D*, and *bFGF* up-regulation in *EFF*-nanotransfected cells at day 1 after nanotransfection ($n = 3$). (**C**) qRT-PCR analysis of *EFF*, *VEGF-D*, and *bFGF* loading in exosomes derived from *EFF*-nanotransfected pMEFs at day 1 ($n = 3$ to 6). (**D**) Immunofluorescence micrographs of *EFF*-nanotransfected cells at day 7. Left to right: nuclear staining [4′,6-diamidino-2-phenylindole (DAPI)], plasmid-tag (Myc-DDK), endothelial marker (vWF), and circled elements in the merged + bright field (BF) *EFF* micrograph highlight co-localization of Myc-DDK and vWF in nanotransfected cells (scale bar, 25 μm). (**E**) In vitro tube formation assay results of sham- and *EFF*-nanotransfected pMEFs and mouse endothelial cells at 5 hours ($n = 4$) (scale bar, 200 μm). (**F** and **G**) Brain perfusion in healthy mice 7 days after intracranial injection of *EFF*- or sham/control-nanotransfected cells with representative tracings for perfusion assessment ($n = 12$). All error bars are shown as SEs. $^*P < 0.05$ and $^{***}P < 0.001$ (one-tailed *t* test). A.U., arbitrary units.

Histological analyses clearly confirmed an increase in vascularity, which may help explain the overall positive impact on intracranial perfusion. As mentioned above, however, note that the enhanced vascularity seen in mice treated with *EFF*-nanotransfected pMEFs relative to control could reflect the combined effect of iEC-directed reprogramming of a proportion of the injected cells and induced vasculogenesis or angiogenesis from preexisting vascular tissue, possibly driven by *EFF*-laden exosomes or other factors.

Notably, portions of immunostained vasculature in the stroke-affected hemisphere of *EFF*-treated mice colocated with the C-terminal Myc-DDK tag associated with the nanotransfected *EFF* factors (fig. S5), suggesting that at least a portion of the nanotransfected pMEFs is structurally involved in the de novo formation of induced vasculature (iVas), intracranially. Given that the average half-life of a transcription factor is <1 day (e.g., Fli1 half-life is ~1.5 hours) (*26*), positive coimmunoreactivity for the Myc-DDK tag and vascular markers at day 21 after stroke (i.e., 15 days post nanotransfection of the *EFF* plasmids) suggests that the *EFF* plasmids are still being actively expressed in some cells and that the iEC phenotype is retained at least by day 15 after *EFF* nanotransfection (i.e., 14 days following intracranial delivery). However, additional studies are needed to confirm whether reprogrammed iECs maintain their phenotype or presence beyond the 15-day time point and whether therapeutic efficacy is directly linked to iEC phenotypic stability and/or nanotransfected cell longevity after injection.

Intracranial injection of *EFF*-nanotransfected fibroblasts attenuates stroke-induced injury

To assess the impact of nanotransfection-driven iVas on the progression of infarct resolution after stroke, we performed magnetic resonance imaging (MRI) 2 days following the MCAO procedure and then again 14 days after stroke (i.e., 7 days after intracranial cell

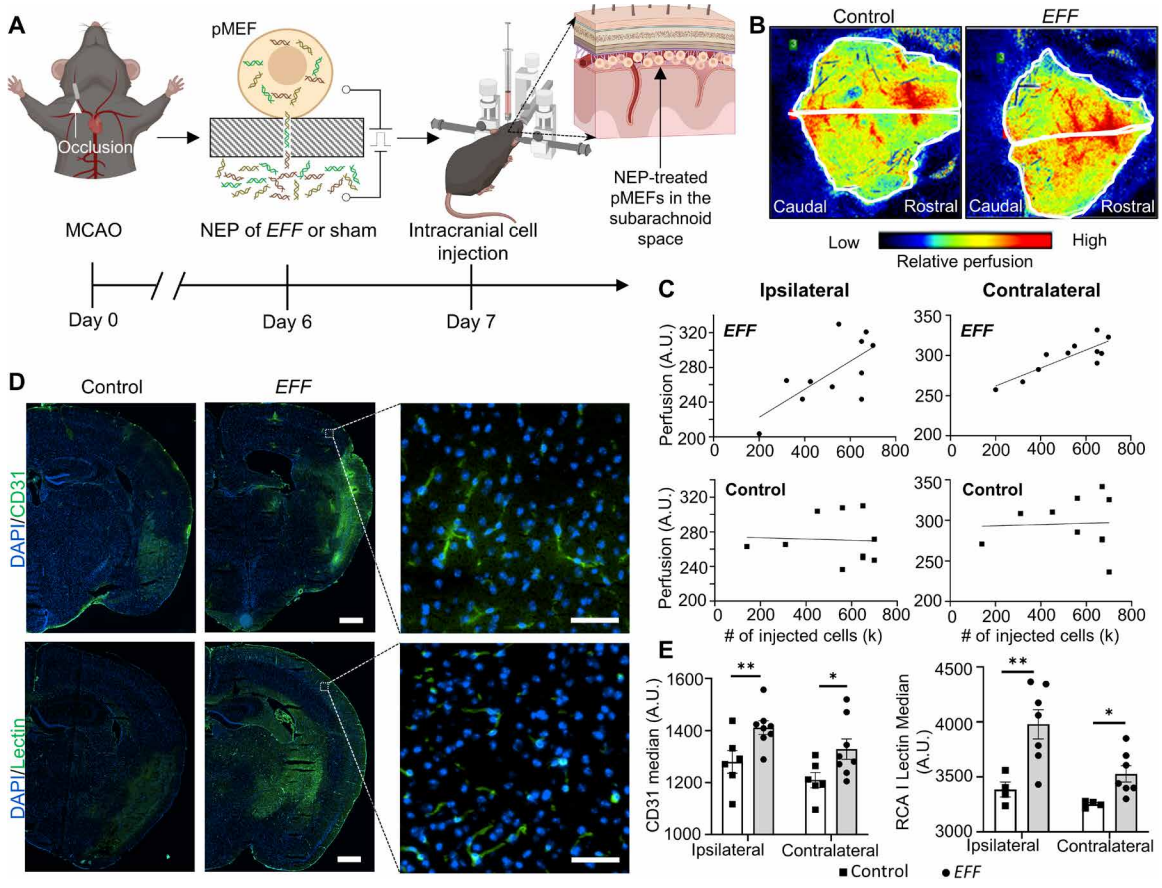

Fig. 2. Intracranial injection of *EFF*-nanotransfected fibroblasts results in increased brain vasculature. (**A**) Schematic diagram of artery occlusion for the induction of ischemic stroke (day 0) and intracranial injection procedure (day 7) delivering *EFF*- or sham-nanotransfected pMEFs to the subarachnoid space of the ipsilateral hemisphere. (**B**) Brain perfusion 21 days after stroke in mice treated with sham- or *EFF*-nanotransfected cells with representative tracings for perfusion assessment. (**C**) Linear regression analysis of the perfusion in the ipsilateral hemisphere versus (top left) number of *EFF*-nanotransfected cells delivered [coefficient of determination (R^2) = 0.480, adj. R^2 = 0.422, P = 0.018, n = 11] and versus (bottom left) number of sham-nanotransfected cells delivered (R^2 = 0.002, adj. R^2 = 0.000, P = 0.894, n = 10). Linear regression analysis of the contralateral hemisphere perfusion versus (top right) number of *EFF*-nanotransfected cells delivered (R^2 = 0.696, adj. R^2 = 0.662, P = 0.001, n = 11) and (bottom right) sham-nanotransfected cells delivered (R^2 = 0.002, adj. R^2 = 0.000, P = 0.906, n = 10). (**D**) Immunofluorescence micrographs of the ipsilateral hemisphere depicting the nuclear stain (DAPI) and endothelial marker (CD31 and RCA I lectin) expression 21 days after stroke in mice treated with sham- or *EFF*-nanotransfected cells (scale bars, 750 μm) with representative higher-magnification insets (scale bars, 50 μm). (**E**) CD31 and RCA I lectin quantification in ipsilateral and contralateral hemispheres (n = 4 to 8). All error bars are shown as SEs. *P < 0.05 and **P < 0.01 (one-tailed t test).

injection) in mice treated with sham- or *EFF*-nanotransfected cells (Fig. 3A). MRI-based visualization of the stroke injury 2 days after MCAO confirmed a right hemisphere MCA territory infarct, with clear compromise of the motor cortex (Fig. 3B). Digital planimetry was performed on the coronal brain images to quantify infarct, ipsilateral, and contralateral hemisphere areas (Fig. 3B). Infarct areas from all slices were summed and multiplied by slice thickness (0.8 mm) to provide infarct volume. Given that stroke-induced swelling can compress healthy contralateral tissue, infarct volume was then corrected for edema-induced swelling, as previously described (*27*). Mice treated with *EFF*-nanotransfected pMEFs demonstrated a trend (P = 0.1) of greater stroke volume reduction compared to mice injected with control pMEFs (Fig. 3C).

Further analysis of confounding factors revealed that stroke volume reduction was significantly affected by the extent of weight loss experienced by the mice following stroke (fig. S6). In stroke patients, weight loss due to malnutrition, for example, has been shown to lead to impaired brain recovery (e.g., alterations in hippocampal plasticity–associated proteins), additional complications (e.g., urinary tract infections), and poorer clinical outcomes (*28*, *29*). In this study, we found that mice with weight loss below 17% correlated with similar levels of spontaneous reduction in infarct volume regardless of treatment (fig. S6). Nevertheless, when weight loss exceeded 17%, we found that intracranial injection of *EFF*-nanotransfected pMEFs led to significantly improved infarct resolution compared to mice treated with sham-nanotransfected pMEFs (Fig. 3D).

Mice treated with *EFF*-nanotransfected fibroblasts show increased neuronal cellularity and reduced astroglial scar formation in the stroke-affected hemisphere

During an ischemic stroke event, a reduction in oxygen and glucose levels induces substantial necrotic neuronal death at the core of the infarct zone. In the penumbra region, in addition to hypoperfusion, excitotoxicity as a consequence of excessive glutamate release results in the activation of programmed cell death pathways such as apoptosis and autophagy, which, in turn, leads to increased cellular

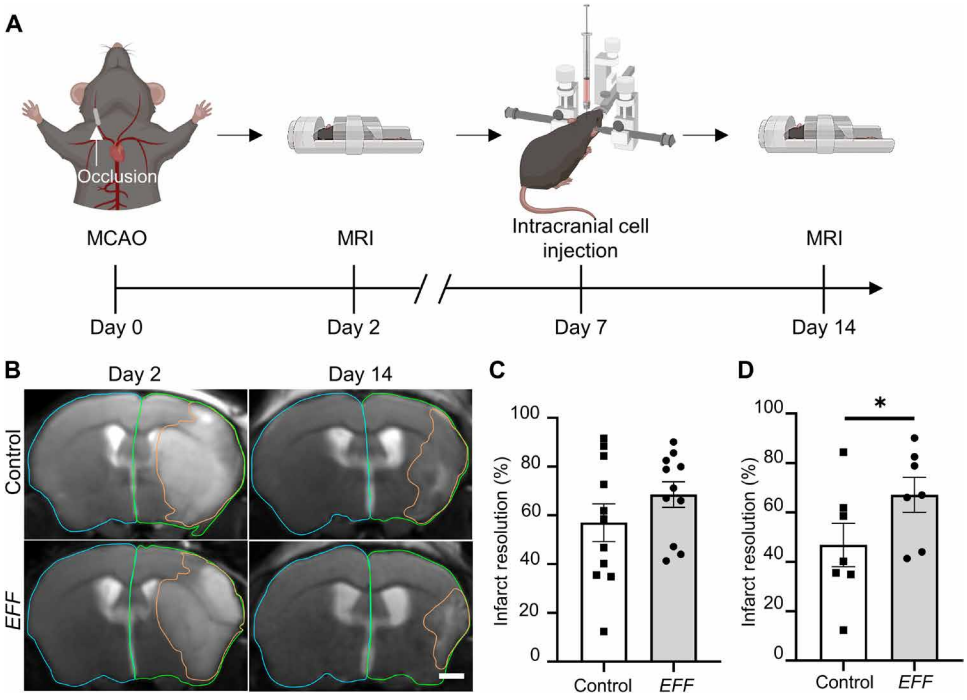

Fig. 3. Enhanced infarct resolution observed in mice treated with *EFF*-nanotransfected fibroblasts. (**A**) Schematic diagram depicting the experimental timeline of MCAO (day 0), intracranial injection (day 7), and MRIs (days 2 and 14). (**B**) T2-weighted MR images 2 and 14 days after stroke with representative tracings for assessment of infarct volume (orange) and hemisphere volumes (green/blue) (scale bar, 1 mm). (**C**) Infarct resolution from days 2 to 14 after stroke in mice treated with sham- or *EFF*-nanotransfected cells ($n = 11$). (**D**) Mice treated with sham- or *EFF*-nanotransfected cells and >17% loss in body weight by intracranial injection (day 7) infarct resolution from days 2 to 14 ($n = 7$). All error bars are shown as SEs. *$P < 0.05$ (one-tailed t test).

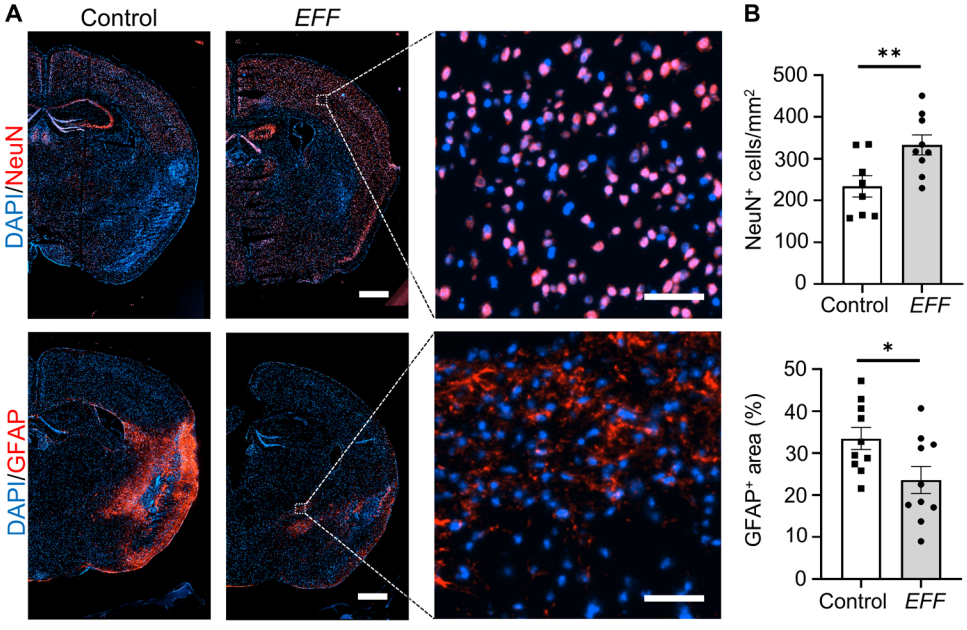

Fig. 4. Mice treated with *EFF*-nanotransfected fibroblasts demonstrate greater neuronal cellularity and less astroglial scar formation. (**A**) Immunofluorescence micrographs of the ipsilateral hemisphere showing nuclear (DAPI), neuronal (NeuN), and astroglial (GFAP) staining 21 days after stroke in mice treated with sham- or *EFF*-nanotransfected cells (scale bars, 750 μm) with representative higher-magnification insets (scale bars, 50 μm). (**B**) NeuN and GFAP quantification in the ipsilateral hemisphere ($n = 8$ to 10). Micrographs and quantification analysis show better preservation of neurons and reduction of astroglial scarring in stroke-affected regions of the brain, including the thalamus; hypothalamus; striatum; and the adjacent prefrontal, parietal, and temporal cortex. All error bars are shown as SEs. *$P < 0.05$ and **$P < 0.01$ (one-tailed t test).

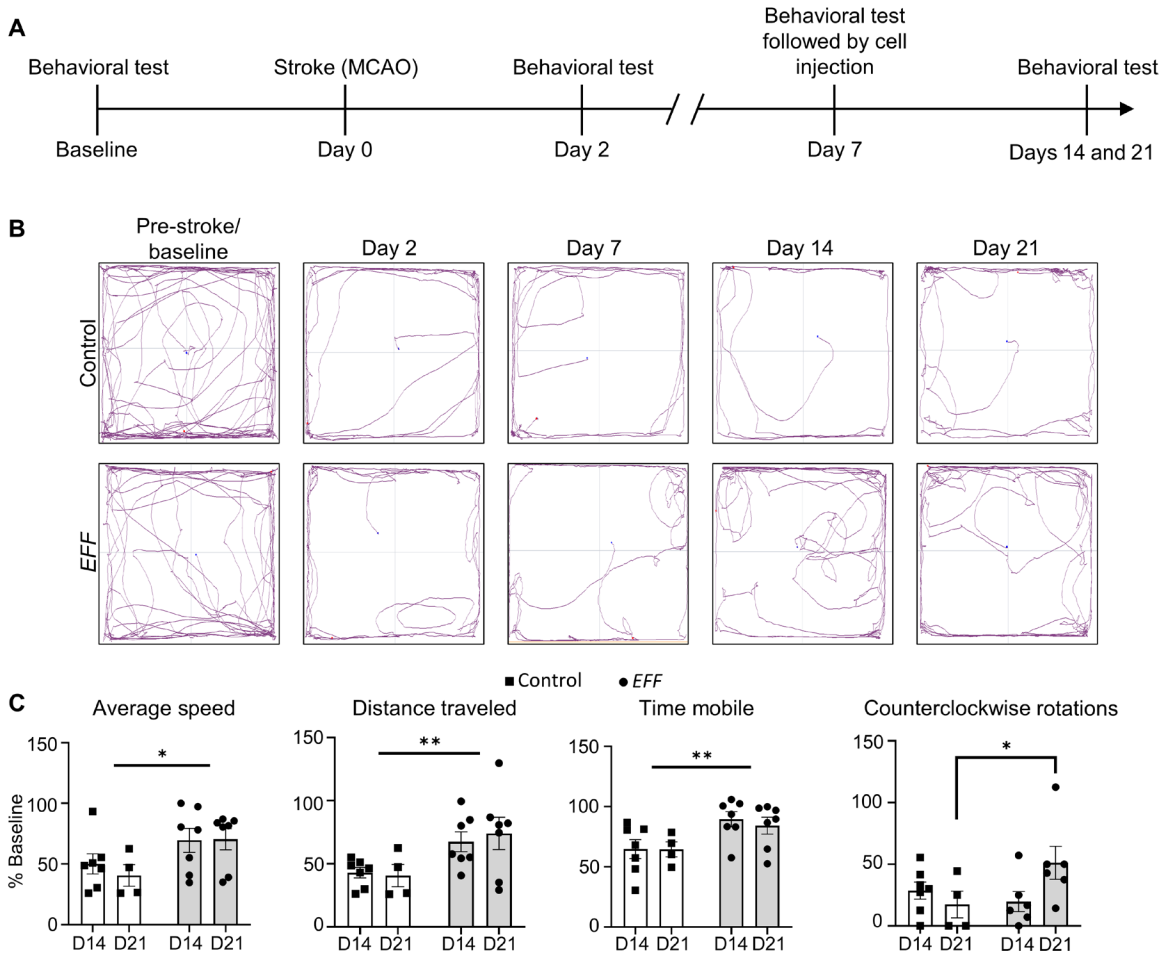

Fig. 5. Enhanced motor function observed in mice injected with *EFF*-nanotransfected fibroblasts. (**A**) Experimental timeline of behavioral tests. (**B**) Track plots depicting mice movement in behavioral tests before and on days 2, 7, 14, and 21 after stroke. (**C**) Individual behavioral parameter quantification after sham- or *EFF*-nanotransfected cell injection for average speed, distance traveled, time mobile, and number of counterclockwise rotations ($n = 4$ to 7). All error bars are shown as SEs. $^{*}P < 0.05$ and $^{**}P < 0.01$ (two-way ANOVA).

death and tissue damage (*30*). Alongside cell death, substantial tissue remodeling is driven by astrocytic hyperproliferation (i.e., reactive astrogliosis) in the peri-infarct zone, which causes glial scar formation and could have a long-term detrimental impact on brain tissue repair/regeneration (*31*). To determine how the post-stroke cellular landscape is affected by the intracranial delivery of *EFF*- or sham-nanotransfected cells, brains were collected 21 days after stroke and processed for immunofluorescence analysis of neuronal and astroglial markers. Quantitative analyses show that compared to controls, mice injected with *EFF*-nanotransfected fibroblasts had a significantly higher count of neurons (i.e., $NeuN^{+}$ cells) (Fig. 4A) and considerably less astroglial scarring in the stroke-affected hemisphere based on reduced glial fibrillary acidic protein (GFAP) immunoreactivity (Fig. 4B). Analysis of additional markers also showed positive immunoreactivity for ionized calcium binding adaptor molecule 1 (Iba-1), confirming the presence of microglia infiltration into the stroke-affected regions 21 days after MCAO (fig. S7) (*32*, *33*).

Intracranial delivery of *EFF*-nanotransfected fibroblasts improves post-stroke sensorimotor outcomes

To evaluate the impact of *EFF*- or sham-nanotransfected cells on the recovery of locomotive abilities after stroke, mice underwent a standard open-field test (Fig. 5A) before stroke (i.e., baseline), after stroke (i.e., days 2 and 7), and after treatment delivery (i.e., days 14 and 21). Ischemic stroke caused marked locomotive impairment at day 2 after MCAO, with continued decline through post-stroke day 7 (Fig. 5, B and C). This decrease in activity and inclination to favor clockwise rotations is consistent with locomotive decline and unilateral side neglect, driven by the stroke lesion (*34*). However, the injection of *EFF*-nanotransfected cells at day 7 after stroke facilitated significant improvement in motility by days 14 and 21 after stroke (i.e., days 8 and 15 after nanotransfection) compared to mice injected with sham-nanotransfected cells (Fig. 5, B and C). Significant differences were detected in multiple parameters, including average speed, traveled distance, time mobile, and counterclockwise rotations, among others (Fig. 5C and fig. S8).

Unilateral neglect affects ~40 to 80% of patients with right hemisphere stroke (*35*, *36*). While some patients experience spontaneous recovery during the acute phase of stroke (*37*), persistence past the acute phase can result in durable impairment (*38*). Our results, however, indicate that the injection of *EFF*-nanotransfected cells could potentially help stem or reverse the progression of unilateral neglect. Together, our results suggest that intracranial deployment of *EFF*-nanotransfected cells can lead to an overall improvement in

gross motor skills in stroke-affected mice. However, additional studies are needed for a more in-depth evaluation of the impact of this potential therapeutic strategy on fine motor skills, which are also markedly affected by the stroke lesion in the motor cortex (*39*, *40*).

CONCLUSIONS

Nonviral approaches to gene/cargo delivery have the potential to facilitate the development of highly translational cell therapies for a wide variety of conditions (*18*, *19*, *41*–*45*). Here, we showed that nonviral nanotransfection of *Etv2*, *Foxc2*, and *Fli1* (*EFF*) into fibroblasts can drive reprogramming-based vasculogenic cell therapies of relevance to ischemic stroke when deployed intracranially. Notably and consistent with previous reports (*46*, *47*), intracranial injection of control fibroblasts does not appear to have an impact on major stroke outcomes, including infarct resolution and locomotive abilities (fig. S9), suggesting that *EFF* nanotransfection was key to driving therapeutic efficacy. Our results indicate that *EFF*-nanotransfected fibroblasts not only exhibited the ability to convert into vascular cells in vitro and in vivo but also released exosomes that could potentially be mediating provasculogenic/angiogenic responses following intracranial delivery into the stroke-affected brain. Previously, we reported that exosomes derived from *EFF*-nanotransfected skin tissue can be used to attenuate necrosis in a mouse model of hindlimb ischemia (*19*). Additional studies, however, are needed to independently trace and evaluate the impact of exosomes derived from *EFF*-nanotransfected fibroblasts on stroke recovery. *EFF* nanotransfection also appears to foment the overexpression of prolymphogenic transcripts, which warrants further investigation within the context of stroke recovery. Intracranial delivery of *EFF*-nanotransfected fibroblasts increased perfusion in a dose-dependent manner, which correlated with increased immunoreactivity for vascular markers in the ipsilateral and contralateral hemispheres. Stroke-induced edema leads to secondary injury that can hinder infarct volume resolution and overall recovery, contributing to increased morbidity and mortality (*48*). Notably, while edema continues to be a considerable hurdle for vascular therapies (*49*), our reprogramming-based approach appears to facilitate infarct volume resolution and thus could potentially offer a promising alternative strategy to vascular therapies. Behavioral analyses revealed significant locomotive recovery in mice treated with *EFF*-nanotransfected cells, both in overall motility (e.g., average speed, traveled distance, and time mobile) and unilateral spatial neglect (i.e., counterclockwise rotations). Histological analyses of the ipsilateral hemisphere 21 days after stroke revealed increased neuronal cellularity and reduced astroglial presence, potentially contributing to improved functional outcomes. Together, our results suggest that provasculogenic cell therapies based on nonviral cellular reprogramming represent a promising strategy for the treatment of ischemic stroke.

METHODS

Experimental design

The objective of this study was to investigate whether the intracranial injection of *EFF*-reprogrammed fibroblasts into a mouse model of ischemic stroke could enhance cerebral vasculature and structural/functional outcomes. All in vitro studies used pMEFs (reference no. PMEF-HL, MilliporeSigma). Sham- and *EFF*-nanotransfected pMEFs were intracranially injected into 10-week-old male C57BL/6 mice 7 days after stroke. Cell and exosome gene expression and loading, brain perfusion, brain vasculature, infarct volume, neuronal cellularity, glial scar formation, and behavioral parameters were analyzed at predetermined time points using qRT-PCR, LSI, MRI, open-field tests, or immunohistology as appropriate. No statistical method was used to predetermine sample size. In vitro and in vivo biological replicates and end points were determined on the basis of statistical significance and/or in accordance with protocols approved by the Laboratory Animal Care and Use Committee at The Ohio State University [Institutional Animal Care and Use Committee (IACUC) no. 2016A00000074-R1 and IACUC no. 2009A0006-R3]. All in vivo data were collected across (four) experimental cohorts with 8 to 12 mice per cohort assigned to sham/control- or *EFF*-nanotransfected fibroblasts treatment in a randomized fashion. An additional cohort of mice received no intracranial injection of fibroblast (i.e., stroke only) for comparison purposes. Previous studies, however, indicate that the intracranial delivery of fibroblasts alone has no significant positive or negative effect on structural or functional recovery in mice following stroke (*46*, *47*). Data were collected, processed, and quantified via automated tools and/or completed by blinded investigators. Successful MCAO and subsequent survival throughout the length of the experiment (21 days) was a prerequisite for inclusion into experimental analysis. Post hoc exclusion criteria included immunomicrographs with observed artifacts and/or statistical outliers (i.e., studentized residual, >3 SDs).

Cell transfection and exosome isolation

A full list of plasmids used can be found in table S1. All plasmids were prepared using a plasmid DNA isolation kit (ZymoPURE; reference no. D4201) per the manufacturer's protocol. DNA concentrations were obtained from NanoDrop 2000c Spectrophotometer (Thermo Fisher Scientific). The cells were then reprogrammed as previously described by Gallego-Perez *et al.* (*18*, *19*) with a few modifications. Briefly, pMEFs (reference no. PMEF-HL, MilliporeSigma) were seeded at a density of ~1.3×10^5 cells/cm^2 on the apical surface of a modified transwell insert (reference no. 3460, Corning Inc.) in Dulbecco's Modified Eagle Medium (DMEM) (reference no. 11965092, Thermo Fisher Scientific) with 10% exosome-depleted fetal bovine serum (reference no. A2720801, Thermo Fisher Scientific) and 1% Non-Essential Amino Acids (NEAA) (reference no. 11140050, Thermo Fisher Scientific). Cells were given 4 to 6 hours to adhere to the nanochanneled membrane before nanotransfection. The *EFF* plasmids were mixed at a 1:1:1 ratio at 0.05 μg/μl each in phosphate-buffered saline (PBS) and loaded into the nanochannels via the basal surface of the transwell, as seen in Fig. 1A, and a pulsed electric field (~27.5 V/mm, 35-ms pulses, 10 pulses) was applied across Au-plated electrodes to nanoporate the cell membrane and electrophoretically drive the plasmids into the cells. pMEFs were nanotransfected with sham (i.e., pCMV6) plasmids at a concentration of 0.15 μg/μl in PBS in an identical manner as described above to serve as control. The cells were then incubated for 16 to 24 hours at 37°C. Conditioned media were collected from each sample, and the cells were detached from the transwell insert using standard processes for downstream procedures (e.g., intracranial injection, RNA extraction, and exosome isolation). Exosomes were isolated from the collected conditioned media using an exosome isolation kit (reference no. 44-783-59, Invitrogen) per the manufacturer's protocol.

In vitro angiogenesis

Angiogenesis potential in *EFF*-nanotransfected cells 7 days after nanotransfection was assessed as previously described by Arnaoutova and Kleinman (*50*). Sham- and *EFF*-nanotransfected pMEFs and mouse endothelial cells (reference no. CRL-2581, American Type Culture Collection) were cultured in EBM-2 supplemented media (reference no. CC-3156, Lonza) for 7 days before the assay. Cells were then harvested and seeded on Cultrex Basement Membrane Matrix (reference no. 3632-001-02, Trevigen) in a 96-well plate and incubated at 37°C. Bright-field images were taken every hour using a Nikon Ti2-E microscope. Data were represented qualitatively ($n = 4$).

Gene expression/loading

Total RNA was extracted from cells and exosomes using TRIzol (reference no. 15596026, Thermo Fisher Scientific) according to the manufacturer's protocol, and cDNAs were generated by RT using SuperScript IV VILO Master Mix (reference no. 11756500, Thermo Fisher Scientific). qRT-PCR was performed using fluorogenic TaqMan primers (Thermo Fisher Scientific) and the Thermo Fisher Scientific QuantStudio 3. For all qRT-PCR procedures, equal amounts of cDNA were used across samples. Mouse *GAPDH* was used as a reference gene in all qRT-PCR reactions. Specific TaqMan primers used in PCR reactions are listed in table S2. Data analysis was performed as previously described by Königshoff *et al.* (*51*). Relative expression (ΔCt) was determined for each sample as $\Delta Ct = Ct^{reference} - Ct^{target}$. Subsequently, relative expression compared to controls (ΔΔCt) was determined for each sample as $\Delta\Delta Ct = \Delta Ct^{treatment} - \text{average}(\Delta Ct^{control})$. ΔΔCt values equate to approximately the logarithm of the fold change.

Animal husbandry

Eight-week-old male C57BL/6 mice were obtained from the Jackson laboratory. Mice were allotted 1 week upon arrival to acclimate to the facilities. Following stroke induction, wetted food and hydrogel (reference no. 70-01-5022; clearh20.com) were provided to mice daily in addition to standard hard pellet food and water to promote nutrition uptake. Mice demonstrating signs of dehydration were given subcutaneous injections of saline warmed to 37°C, no more than three times within a 24-hour period. All animal experiments were performed in accordance with protocols approved by the Laboratory Animal Care and Use Committee at The Ohio State University (IACUC no. 2016A00000074-R1 and IACUC no. 2009A0006-R3).

MCAO stroke model

Transient focal cerebral ischemia was induced in male C57BL/6 mice (aged 9 weeks) (the Jackson laboratory, Bar Harbor, ME, USA) by the intraluminal suture method of MCAO. Mice were anesthetized by inhaled isoflurane (induced at 5%; maintained at 1.5 to 2%), and their body temperature and respiration were monitored. Following permanent distal ligation of the right external carotid artery, a 6-0 nylon monofilament suture with silicon tip occluder was directed to the common carotid bifurcation and advanced into the right internal carotid artery to the origin of the MCA. Successful MCAO was validated by Laser Doppler Flowmetry (Moor Instruments, Wilmington, DE, USA). Mice were allowed to recover from anesthesia during occlusion. After 30 min of MCAO, mice were reanesthetized, and the occluder was removed to enable reperfusion. Successful MCAO and subsequent survival throughout the length of the experiment (21 days) was a prerequisite for inclusion into experimental analysis.

Intracranial cell delivery

Cells nanotransfected with sham or *EFF* plasmids were delivered via stereotaxic injection (Motorized Stereotaxic with Robot Drill and Injection; Stoelting, Wood Dale, IL, USA) to target the subarachnoid space above the stroke-affected S1/M1 cortex [coordinates from bregma: −0.1 mm, antero-posterior (AP); +1.5 mm, mediolateral (ML); −0.2 mm, dorso-ventral (DV)]. At 7 days after MCAO, mice were anesthetized with isoflurane (induced at 5%; maintained at 1.5 to 2%). With the head secured by a stereotactic frame, the skull was exposed. A 10-μl Hamilton syringe connected to a motorized drill and nano-injector (Robot Drill and Injection Bundle; Stoelting, Wood Dale, IL, USA) delivered an average of ~500,000 sham- or *EFF*-nanotransfected cells in 8 μl of standard DMEM at a rate of 0.25 μl/min. Cells were injected 1 day after nanotransfection, when marked *EFF* gene expression/loading was observed in *EFF*-nanotransfected cells and corresponding derived exosomes, and before observed iEC fate conversion in vitro (Fig. 1). Therefore, no success criterion for iEC fate conversion was used before cell injection in this study.

Magnetic resonance imaging

T2-weighted MR brain imaging was performed using 9.4-T MRI (Bruker BioSpec 94/30; Ettlingen, Germany) at day 2 after MCAO to confirm stroke and again at day 14 to evaluate evolution of stroke volume. Mice were anesthetized by inhaled isoflurane (induced at 5%; maintained at 1.5 to 2%), and respiration was monitored for the duration of imaging, which is approximately 30 min. Following localizer scans, a T2-weighted gradient echo technique with rapid acquisition with relaxation enhancement sequence providing eight echo train length was applied (field of view, 30 mm by 30 mm; acquisition matrix, 256 by 256; repetition time, 3500 ms; echo time, 46.924 ms; flip angle, 180°; images in acquisition, 19; resolution, 8.533 pixels/mm; and number of averages, 2). Mice without MCA territory infarction at day 2 were excluded from the study.

Stroke volume analysis

Infarct volumes at days 2 and 14 after stroke were calculated from raw MR images converted to Digital Imaging and Communications in Medicine format using OsiriX MD version 10.0.5 (Pixmeo, Bernex, Switzerland). In OsiriX, image contrast was adjusted and matched across all coronal brain images, after which digital planimetry was performed by a blinded observer to quantify infarct area. Infarct areas from all slices were summed and multiplied by slice thickness (0.8 mm) to provide infarct volume. Given that stroke-induced swelling can compress healthy contralateral tissue, infarct volume was then corrected for edema-induced swelling, as previously described (*27*). Because MRIs from post-stroke day 14 exhibited no edema, day 14 infarct volumes and edema-corrected infarct volumes were identical.

Percent reduction of edema-corrected stroke volume from post-stroke days 2 to 14 was calculated as follows

$$[(\text{post-stroke day 2 volume} - \text{post-stroke day 14 volume}) / \text{post-stroke day 2 volume}] \times 100$$

Analysis presented two significant confounding factors (fig. S6); stroke volume reduction from post-stroke days 2 to 14 was significantly

affected by the degree of weight loss observed at post-stroke day 7. Albeit daily efforts to enhance nutritional uptake in mice after stroke were made, mouse-to-mouse variances in malnutrition, quantified by percent body weight loss, were still observed. Malnutrition in stroke patients has been shown to lead to impaired brain recovery mechanisms (e.g., alteration hippocampal plasticity–associated proteins), additional complications (e.g., urinary tract infections), and ultimately poorer outcomes in stroke patients (*28*, *29*). Because loss in body weight at post-stroke day 7 ranged between 0 and 35%, mice were segregated into two subgroups at the approximate range midpoint (body weight loss of <17 or >17%) for further analysis.

Behavioral analysis

Spontaneous sensorimotor activity was assessed at baseline (pre-MCAO) and again at days 2, 7, 14, and 21 after stroke. Mice were placed in the center of an open field with dimensions 1 m by 1 m and allowed to freely roam for 5 min. An overhead camera recorded the tests for subsequent automated analysis by ANY-maze video tracking software (version 4.99; Stoelting, Wood Dale, IL, USA), where calculated parameters included total distance traveled (in m), average speed (in m/s), total time mobile (in s), number of total rotations, number of clockwise rotations, and number of counterclockwise rotations. Each calculated parameter value on days 2, 7, 14, and 21 after stroke for each mouse was normalized to respective baseline measurements (e.g., [d21 average speed/baseline average speed] × 100) to derive percent baseline values. Tests were performed in the morning hours, in a room controlled for light and noise, and always before scheduled anesthetic events (i.e., MCAO, MRI, and cranial injection).

Laser speckle imaging

Brain perfusion in healthy mice was assessed 7 days after intracranial cell injection, immediately before euthanasia. Brain perfusion in stroke-affected mice was assessed 21 days after stroke, immediately before euthanasia. Mice were anesthetized with isoflurane (induced at 5%; maintained at 1.5 to 2%). The skull was exposed via surgical removal of the skin, cleaned, and kept wet with saline. LSI was performed using a PeriCam PSI high-resolution camera (Perimed) operating on Pimsoft software with the following settings: required height, 10 cm; measurement area, 1.5 cm^2; point density, high; frame rate, 6 images per second; duration, number of images; number of images, 20; and record with averaging, 8. Digital planimetry was performed by a blinded observer to extract average perfusion values for ipsilateral and contralateral hemispheres. Changes in brain perfusion versus the number of nanotransfected cells injected were compared using linear regression analysis.

Immunostaining of cells and tissue

All cell and tissue immunostaining were carried out using specific antibodies and standard procedures. Briefly, sham- and *EFF*-nanotransfected cells were fixed 7 days after nanotransfection with 10% formalin, blocked with 10% normal goat serum, and incubated with specific primary antibodies at +4°C for 16 hours and subsequent fluorescence-tagged secondary antibodies at room temperature for 1 hour to visualize target signal (table S3). Brain tissue was harvested 21 days after stroke, coronally sliced using a brain matrix, and frozen at −80°C in OCT (reference no. 4585, Thermo Fisher Scientific). OCT-embedded brain tissue was sectioned at 10 μm and mounted to charged microscopy slides. Day 2 MRIs were referenced to select tissue sections that best represented the stroke centroid. Tissue sections were fixed in cold methanol, blocked with 10% normal goat serum and/or mouse-on-mouse blocking reagent, and incubated with specific primary antibodies at +4°C for 16 hours and subsequent fluorescence-tagged secondary antibodies at room temperature for 1 hour to visualize target signal (table S3). For endothelial cell staining with fluorescein-conjugated RCA I lectin, tissues were incubated in RCA I at room temperature for 20 min. Stained cells and tissue sections were imaged using Nikon Ti2-E microscope operating on NIS-Elements AR version 5.20. All immunocytochemistry imaging was completed using 20× and 40× objective lens. Full brain immunohistology images were compiled using an automated image stitching feature using 63 (9 × 7) individual images captured from a 10× objective lens. High-magnification immunohistology images were captured using a 40× objective lens.

Image analysis

Stroke infarct volume ranged between ~3 and 22% total brain volume, as calculated in the day 2 MRI. Immunohistochemistry (IHC) quantification was completed using single IHC sections that best represented each mouse stroke centroid, as informed by the MR images. All quantification was completed using ImageJ Fiji software (*52*). Briefly, uniform thresholds were applied to all images. All quantification was performed using automated methods and/or by a blinded observer, as appropriate. Digital planimetry was performed by a blinded observer to define regions of interest (e.g., ipsilateral hemisphere) for downstream histology quantification. The median $CD31^+$ and $lectin^+$ signal in each sample was quantified for endothelial cell quantification. The number of colocalized $NeuN^+$ and 4′,6-diamidino-2-phenylindole–positive ($DAPI^+$) cells were calculated to determine the total number of mature neurons. Digital planimetry was performed by a blinded observer on remnant $GFAP^+$ signal to determine the area of enhanced astroglial presence. Colocalization of $Myc\text{-}DDK^+$ and Von Willebrand Wactor $(vWF)^+$ blood vessels were identified by a blinded observer and averaged across three locations per sample. Histology samples having tears in the tissue that provided insufficient area for proper calculation and/or immunostaining artifacts such as excessive background were removed from downstream statistical analyses.

Enzyme-linked immunosorbent assay

Protein expression/levels for key vasculogenic factors including vascular endothelial growth factor A (VEGF-A), VEGF-D, and basic fibroblast growth factor (bFGF) was quantified via enzyme-linked immunosorbent assay (ELISA) using the following commercially available kits as per the manufacturer's instructions: VEGF (reference no. DY493, R&D Systems), VEGF-D (reference no. DY469, R&D Systems), and bFGF2 (ref. no. DY3139-05, R&D Systems). Sham- and *EFF*-nanotransfected pMEFs and corresponding exosomes were processed to isolate total protein using a lysis buffer containing radioimmunoprecipitation assay buffer (reference no. 89900, Thermo Fisher Scientific), cOmplete Protease Inhibitor Cocktail (reference no. 4693116001, Roche), phosphatase inhibitor cocktail 2 (reference no. P5726-1, Sigma-Aldrich), and 1 mM phenylmethylsulfonyl fluoride. All samples were incubated in lysis buffer for 15 min at 4°C and overnight at −20°C; the samples were subsequently gently vortexed for 15 min and centrifuged at 10,000 rpm and 4°C for 30 min before protein isolation. Protein concentration for all

samples was determined via a standard Bradford protein assay (reference no. 500006, Bio-Rad) following the vendor's protocol, and these values were used to normalize protein loading for each ELISA assays.

Statistical analysis

All data are reported as means and SEs. Statistical analyses were completed using SigmaPlot version 14.0. To test the experimental hypothesis and determine whether *EFF*-transfection/intracranial injection of *EFF*-nanotransfected fibroblasts improved prespecified parameters, comparisons between groups were performed using linear regression analyses, one-tailed *t* tests, two-way analyses of variance (ANOVAs), or associated nonparametric test equivalents on 3 to 11 biological replicates, as appropriate. Statistical outliers (>3 studentized SDs) were excluded from respective analyses. Tables S4 and S5 detail null hypothesis testing (e.g., *t* test) results. Statistical significance was defined as $P < 0.05$.

SUPPLEMENTARY MATERIALS

Supplementary material for this article is available at http://advances.sciencemag.org/cgi/content/full/7/12/eabd4735/DC1

View/request a protocol for this paper from *Bio-protocol*.

REFERENCES AND NOTES

1. W. Johnson, O. Onuma, M. Owolabi, S. Sachdev, Stroke: A global response is needed. *Bull. World Health Organ.* **94**, 634 (2016).
2. S. S. Virani, A. Alonso, E. J. Benjamin, M. S. Bittencourt, C. W. Callaway, A. P. Carson, A. M. Chamberlain, A. R. Chang, S. Cheng, F. N. Delling, L. Djousse, M. S. V. Elkind, J. F. Ferguson, M. Fornage, S. S. Khan, B. M. Kissela, K. L. Knutson, T. W. Kwan, D. T. Lackland, T. T. Lewis, J. H. Lichtman, C. T. Longenecker, M. S. Loop, P. L. Lutsey, S. S. Martin, K. Matsushita, A. E. Moran, M. E. Mussolino, A. M. Perak, W. D. Rosamond, G. A. Roth, U. K. A. Sampson, G. M. Satou, E. B. Schroeder, S. H. Shah, C. M. Shay, N. L. Spartano, A. Stokes, D. L. Tirschwell, L. B. VanWagner, C. W. Tsao; American Heart Association Council on Epidemiology and Prevention Statistics Committee and Stroke Statistics Subcommittee, Heart disease and stroke statistics—2020 update: A report from the american heart association. *Circulation* **141**, CIR0000000000000757 (2020).
3. National Institute of Neurological Disorders and Stroke rt-PA Stroke Study Group, Tissue plasminogen activator for acute ischemic stroke. *N. Eng. J. Med.* **333**, 1581–1588 (1995).
4. R. G. Nogueira, A. P. Jadhav, D. C. Haussen, A. Bonafe, R. F. Budzik, P. Bhuva, D. R. Yavagal, M. Ribo, C. Cognard, R. A. Hanel, C. A. Sila, A. E. Hassan, M. Millan, E. I. Levy, P. Mitchell, M. Chen, J. D. English, Q. A. Shah, F. L. Silver, V. M. Pereira, B. P. Mehta, B. W. Baxter, M. G. Abraham, P. Cardona, E. Veznedaroglu, F. R. Hellinger, L. Feng, J. F. Kirmani, D. K. Lopes, B. T. Jankowitz, M. R. Frankel, V. Costalat, N. A. Vora, A. J. Yoo, A. M. Malik, A. J. Furlan, M. Rubiera, A. Aghaebrahim, J. M. Olivot, W. G. Tekle, R. Shields, T. Graves, R. J. Lewis, W. S. Smith, D. S. Liebeskind, J. L. Saver, T. G. Jovin, Thrombectomy 6 to 24 hours after stroke with a mismatch between deficit and infarct. *N. Eng. J. Med.* **378**, 11–21 (2018).
5. W. Hacke, M. Kaste, E. Bluhmki, M. Brozman, A. Dávalos, D. Guidetti, V. Larrue, K. R. Lees, Z. Medeghri, T. Machnig, D. Schneider, R. von Kummer, N. Wahlgren, D. Toni; ECASS Investigators, Thrombolysis with alteplase 3 to 4.5 hours after acute ischemic stroke. *N. Eng. J. Med.* **359**, 1317–1329 (2008).
6. M. Krause, T. G. Phan, C. G. Sobey, H. Ma, R. Lim, Cell-based therapies for stroke: Are we there yet? *Front. Neurol.* **10**, 656 (2019).
7. L. Fletcher, S. Kohli, S. M. Sprague, R. A. Scranton, S. A. Lipton, A. Parra, D. F. Jimenez, M. Digicaylioglu, Intranasal delivery of erythropoietin plus insulin-like growth factor–I for acute neuroprotection in stroke. *J. Neurosurg.* **111**, 164–170 (2009).
8. J. Silver, J. H. Miller, Regeneration beyond the glial scar. *Nat. Rev. Neurosci.* **5**, 146–156 (2004).
9. L.-R. Zhao, A. Willing, Enhancing endogenous capacity to repair a stroke-damaged brain: An evolving field for stroke research. *Prog. Neurobiol.* **163-164**, 5–26 (2018).
10. P. R. Thored, J. Wood, A. Arvidsson, J. Cammenga, Z. Kokaia, O. Lindvall, Long-term neuroblast migration along blood vessels in an area with transient angiogenesis and increased vascularization after stroke. *Stroke* **38**, 3032–3039 (2007).
11. R. Tamarat, J. S. Silvestre, S. le Ricousse-Roussanne, V. Barateau, L. Lecomte-Raclet, M. Clergue, M. Duriez, G. Tobelem, B. I. Lévy, Impairment in ischemia-induced neovascularization in diabetes: Bone marrow mononuclear cell dysfunction and therapeutic potential of placenta growth factor treatment. *Am. J. Pathol.* **164**, 457–466 (2004).
12. M. Rodrigues, V. W. Wong, R. C. Rennert, C. R. Davis, M. T. Longaker, G. C. Gurtner, Progenitor cell dysfunctions underlie some diabetic complications. *Am. J. Pathol.* **185**, 2607–2618 (2015).
13. A. S. Lee, C. Tang, M. S. Rao, I. L. Weissman, J. C. Wu, Tumorigenicity as a clinical hurdle for pluripotent stem cell therapies. *Nat. Med.* **19**, 998–1004 (2013).
14. T. Vierbuchen, M. Wernig, Direct lineage conversions: Unnatural but useful? *Nat. Biotechnol.* **29**, 892–907 (2011).
15. H. Okano, M. Nakamura, K. Yoshida, Y. Okada, O. Tsuji, S. Nori, E. Ikeda, S. Yamanaka, K. Miura, Steps toward safe cell therapy using induced pluripotent stem cells. *Circ. Res.* **112**, 523–533 (2013).
16. A. J. Mellott, M. L. Forrest, M. S. Detamore, Physical non-viral gene delivery methods for tissue engineering. *Ann. Biomed. Eng.* **41**, 446–468 (2013).
17. P. E. Boukany, A. Morss, W. C. Liao, B. Henslee, H. C. Jung, X. Zhang, B. Yu, X. Wang, Y. Wu, L. Li, K. Gao, X. Hu, X. Zhao, O. Hemminger, W. Lu, G. P. Lafyatis, L. J. Lee, Nanochannel electroporation delivers precise amounts of biomolecules into living cells. *Nat. Nanotechnol.* **6**, 747–754 (2011).
18. D. Gallego-Perez, J. J. Otero, C. Czeisler, J. Ma, C. Ortiz, P. Gygli, F. P. Catacutan, H. N. Gokozan, A. Cowgill, T. Sherwood, S. Ghatak, V. Malkoc, X. Zhao, W. C. Liao, S. Gnyawali, X. Wang, A. F. Adler, K. Leong, B. Wulff, T. A. Wilgus, C. Askwith, S. Khanna, C. Rink, C. K. Sen, L. J. Lee, Deterministic transfection drives efficient nonviral reprogramming and uncovers reprogramming barriers. *Nanomedicine* **12**, 399–409 (2016).
19. D. Gallego-Perez, D. Pal, S. Ghatak, V. Malkoc, N. Higuita-Castro, S. Gnyawali, L. Chang, W. C. Liao, J. Shi, M. Sinha, K. Singh, E. Steen, A. Sunyecz, R. Stewart, J. Moore, T. Ziebro, R. G. Northcutt, M. Homsy, P. Bertani, W. Lu, S. Roy, S. Khanna, C. Rink, V. B. Sundaresan, J. J. Otero, L. J. Lee, C. K. Sen, Topical tissue nano-transfection mediates non-viral stroma reprogramming and rescue. *Nat. Nanotechnol.* **12**, 974–979 (2017).
20. S. Lee, T. A. Vuong, X. Wen, H. J. Jeong, H. K. So, I. Kwon, J. S. Kang, H. Cho, Methylation determines the extracellular calcium sensitivity of the leak channel NALCN in hippocampal dentate granule cells. *Exp. Mol. Med.* **51**, 1–14 (2019).
21. B. H. Dobkin, S. T. Carmichael, The specific requirements of neural repair trials for stroke. *Neurorehabil. Neural Repair* **30**, 470–478 (2016).
22. C. Iadecola, J. Anrather, The immunology of stroke: From mechanisms to translation. *Nat. Med.* **17**, 796–808 (2011).
23. N. G. Ordóñez, Immunohistochemical endothelial markers: A review. *Adv Anat Pathol* **19**, 281–295 (2012).
24. E. A. Salegio, H. Streeter, N. Dube, P. Hadaczek, L. Samaranch, A. P. Kells, W. S. Sebastian, Y. Zhai, J. Bringas, T. Xu, J. Forsayeth, K. S. Bankiewicz, Distribution of nanoparticles throughout the cerebral cortex of rodents and non-human primates: Implications for gene and drug therapy. *Front. Neuroanat.* **8**, 9 (2014).
25. B. Sweetman, A. A. Linninger, Cerebrospinal fluid flow dynamics in the central nervous system. *Ann. Biomed. Eng.* **39**, 484–496 (2011).
26. X. K. Zhang, D. K. Watson, The FLI-1 transcription factor is a short-lived phosphoprotein in T cells. *J. Biochem.* **137**, 297–302 (2005).
27. I. Loubinoux, A. Volk, J. Borredon, S. Guirimand, B. Tiffon, J. Seylaz, P. Méric, Spreading of vasogenic edema and cytotoxic edema assessed by quantitative diffusion and T2 magnetic resonance imaging. *Stroke* **28**, 419–427 (1997).
28. A.-C. Jönsson, I. Lindgren, B. Norrving, A. Lindgren, Weight loss after stroke: A population-based study from the Lund Stroke Register. *Stroke* **39**, 918–923 (2008).
29. S. D. Bouziana, K. Tziomalos, Malnutrition in patients with acute stroke. *J. Nutrit. Metab.* **2011**, 1–7 (2011).
30. A. Datta, D. Sarmah, L. Mounica, H. Kaur, R. Kesharwani, G. Verma, P. Veeresh, V. Kotian, K. Kalia, A. Borah, X. Wang, K. R. Dave, D. R. Yavagal, P. Bhattacharya, Cell death pathways in ischemic stroke and targeted pharmacotherapy. *Transl. Stroke Res.* **11**, 1185–1202 (2020).
31. N. R. Sims, W. P. Yew, Reactive astrogliosis in stroke: Contributions of astrocytes to recovery of neurological function. *Neurochem. Int.* **107**, 88–103 (2017).
32. L. Huang, Z. B. Wu, Q. ZhuGe, W. M. Zheng, B. Shao, B. Wang, F. Sun, K. Jin, Glial scar formation occurs in the human brain after ischemic stroke. *Int. J. Med. Sci.* **11**, 344–348 (2014).
33. M. Nedergaard, U. Dirnagl, Role of glial cells in cerebral ischemia. *Glia* **50**, 281–286 (2005).
34. G. Nys, M. J. E. van Zandvoort, P. L. M. de Kort, H. B. van der Worp, B. P. W. Jansen, A. Algra, E. H. F. de Haan, L. J. Kappelle, The prognostic value of domain-specific cognitive abilities in acute first-ever stroke. *Neurology* **64**, 821–827 (2005).
35. P. M. Pedersen, H. S. Jørgensen, H. Nakayama, H. O. Raaschou, T. S. Olsen, Hemineglect in acute stroke-incidence and prognostic implications: The Copenhagen Stroke Study1. *Am. J. Phys. Med. Rehabil.* **76**, 122–127 (1997).
36. J. Ringman, J. Saver, R. Woolson, W. Clarke, H. Adams, Frequency, risk factors, anatomy, and course of unilateral neglect in an acute stroke cohort. *Neurology* **63**, 468–474 (2004).

37. G. Gainotti, Les manifestations de negligence et d'inattention pour l'hemispace. *Cortex* **4**, 64–91 (1968).
38. L. Pizzamiglio, C. Bergego, P. Halligan, V. Homberg, I. Robertson, E. Weber, B. Wilson, P. Zoccolotti, G. Deloche, Factors affecting the clinical measurement of visuo-spatial neglect. *Behav. Neurol.* **5**, 233–240 (1992).
39. K. L. Schaar, M. M. Brenneman, S. I. Savitz, Functional assessments in the rodent stroke model. *Exp. Transl. Stroke Med.* **2**, 13 (2010).
40. T. Schallert, D. Adkins, *Primer on Cerebrovascular Diseases* (Elsevier, 2017), pp. 355–360.
41. Z. Fei, Y. Wu, S. Sharma, D. Gallego-Perez, N. Higuita-Castro, D. Hansford, J. J. Lannutti, L. J. Lee, Gene delivery to cultured embryonic stem cells using nanofiber-based sandwich electroporation. *Anal. Chem.* **85**, 1401–1407 (2013).
42. Y. Wu, M. C. Terp, K. J. Kwak, D. Gallego-Perez, S. P. Nana-Sinkam, L. J. Lee, Surface-mediated nucleic acid delivery by lipoplexes prepared in microwell arrays. *Small* **9**, 2358–2367 (2013).
43. N. Higuita-Castro, D. Gallego-Perez, K. Love, M. R. Sands, G. Kaletunç, D. J. Hansford, Soft lithography-based fabrication of biopolymer microparticles for nutrient microencapsulation. *Indust. Biotechnol.* **8**, 365–371 (2012).
44. L. Diaz-Starokozheva, D. Das, X. Gu, J. T. Moore, L. R. Lemmerman, I. Valerio, H. M. Powell, N. Higuita-Castro, M. R. Go, A. F. Palmer, D. Gallego-Perez, Early intervention in ischemic tissue with oxygen nanocarriers enables successful implementation of restorative cell therapies. *Cell. Mol. Bioeng.* **13**, 435–446 (2020).
45. J. T. Moore, C. G. Wier, L. R. Lemmerman, L. Ortega-Pineda, D. J. Dodd, W. R. Lawrence, S. Duarte-Sanmiguel, K. Dathathreya, L. Diaz-Starokozheva, H. N. Harris, C. K. Sen, I. L. Valerio, N. Higuita-Castro, W. D. Arnold, S. J. Kolb, D. Gallego-Perez, Nanochannel-based poration drives benign and effective nonviral gene delivery to peripheral nerve tissue. *Adv. Biosyst.* **4**, e2000157 (2020).
46. Y. Jin, J. S. Lee, J. Kim, S. Min, S. Wi, J. H. Yu, G.-E. Chang, A.-N. Cho, Y. Choi, D.-H. Ahn, S.-R. Cho, E. Cheong, Y. G. Kim, H.-P. Kim, Y. Kim, D. S. Kim, H. W. Kim, Z. Quan, H.-C. Kang, S. W. Cho, Three-dimensional brain-like microenvironments facilitate the direct reprogramming of fibroblasts into therapeutic neurons. *Nat. Biomed. Eng.* **2**, 522–539 (2018).
47. S.-J. Chen, C. M. Chang, S. K. Tsai, Y. L. Chang, S. J. Chou, S. S. Huang, L. K. Tai, Y. C. Chen, H. H. Ku, H. Y. Li, S. H. Chiou, Functional improvement of focal cerebral ischemia injury by subdural transplantation of induced pluripotent stem cells with fibrin glue. *Stem Cells Dev.* **19**, 1757–1767 (2010).
48. J. A. Stokum, V. Gerzanich, J. M. Simard, Molecular pathophysiology of cerebral edema. *J. Cereb. Blood Flow Metab.* **36**, 513–538 (2016).
49. A. Marmarou, A review of progress in understanding the pathophysiology and treatment of brain edema. *Neurosurg. Focus* **22**, E1 (2007).
50. I. Arnaoutova, H. K. Kleinman, In vitro angiogenesis: Endothelial cell tube formation on gelled basement membrane extract. *Nat. Protoc.* **5**, 628–635 (2010).
51. M. Königshoff, M. Kramer, N. Balsara, J. Wilhelm, O. V. Amarie, A. Jahn, F. Rose, L. Fink, W. Seeger, L. Schaefer, A. Günther, O. Eickelberg, WNT1-inducible signaling protein–1 mediates pulmonary fibrosis in mice and is upregulated in humans with idiopathic pulmonary fibrosis. *J. Clin. Invest.* **119**, 772–787 (2009).
52. J. Schindelin, I. Arganda-Carreras, E. Frise, V. Kaynig, M. Longair, T. Pietzsch, S. Preibisch, C. Rueden, S. Saalfeld, B. Schmid, J.-Y. Tinevez, D. J. White, V. Hartenstein, K. Eliceiri, P. Tomancak, A. Cardona, Fiji: an open-source platform for biological-image analysis. *Nat. Methods* **9**, 676–682 (2012).
53. S. De Val, B. L. Black, Transcriptional control of endothelial cell development. *Dev. Cell* **16**, 180–195 (2009).
54. J. Giddings, S. Hogg, I. Legg, I. Hughes, The relationship between von Willebrand factor antigen and fibronectin in human plasma, endothelial cells and fibroblasts in culture. *Thromb. Res.* **44**, 291–301 (1986).

Acknowledgments: We thank the Small Animal Imaging core at The Ohio State University Wexner Medical Center for MRI acquisition. Illustrations in Figs. 1 to 3 were created with BioRender.com. **Funding:** This work was funded by New Innovator Award DP2EB028110 to D.G.-P. and R21NS099869 to D.G.-P./C.R./S.K. Additional partial support was provided by awards P30-NS045758 to D.M.M., R01NS085272 to C.R./S.K., and R01NS042617 to C.K.S. **Author contributions:** Cell nanotransfection and downstream analyses were conducted by L.R.L., N.H.-C., J.T.M., D.A.-C., M.A.R.-B., A.S.-P., L.W., I.B.R., A.J.M., S.D.-S., L.O.-P., G.P.G.-V., and D.G.-P. Stroke studies were conducted and overseen by L.R.L., M.H.H.B., J.T.M., H.N.H., S.G., W.L., D.M.M., W.D.A., S.M.N., C.K.S., S.K., C.R., and D.G.-P. The manuscript was written by L.R.L. and D.G.-P. with feedback from all coauthors. **Competing interests:** C.K.S. serves as a scientific advisor and has financial interest in Medeoryx, a start-up company to which *EFF* tissue nanotransfection technology has been licensed by Ohio State. C.K.S. and D.G.-P. are inventors on a patent related to this work filed by Ohio State Innovation Foundation (no. PCT/US2017/067631; filed 20 December 2017, published 28 June 2018). The authors declare that they have no other competing interests. **Data and materials availability:** All data needed to evaluate the conclusions in the paper are present in the paper and/or the Supplementary Materials. The datasets generated and/or analyzed during the current study are available at https://doi.org/10.5061/dryad.qrfj6q5dw. Additional data related to this paper may be requested from the authors.

Submitted 23 June 2020
Accepted 22 January 2021
Published 19 March 2021
10.1126/sciadv.abd4735

Citation: L. R. Lemmerman, M. H. H. Balch, J. T. Moore, D. Alzate-Correa, M. A. Rincon-Benavides, A. Salazar-Puerta, S. Gnyawali, H. N. Harris, W. Lawrence, L. Ortega-Pineda, L. Wilch, I. B. Risser, A. J. Maxwell, S. Duarte-Sanmiguel, D. Dodd, G. P. Guio-Vega, D. M. McTigue, W. D. Arnold, S. M. Nimjee, C. K. Sen, S. Khanna, C. Rink, N. Higuita-Castro, D. Gallego-Perez, Nanotransfection-based vasculogenic cell reprogramming drives functional recovery in a mouse model of ischemic stroke. *Sci. Adv.* **7**, eabd4735 (2021).

ScienceAdvances

Nanotransfection-based vasculogenic cell reprogramming drives functional recovery in a mouse model of ischemic stroke

Luke R. LemmermanMaria H. H. BalchJordan T. MooreDiego Alzate-CorreaMaria A. Rincon-BenavidesAna Salazar-PuertaSurya GnyawaliHallie N. HarrisWilliam LawrenceLilibeth Ortega-PinedaLauren WilchIan B. RisserAidan J. MaxwellSilvia Duarte-SanmiguelDaniel DoddGina P. Guio-VegaDana M. McTigueW. David ArnoldShahid M. NimjeeChandan K. SenSavita KhannaCameron RinkNatalia Higuita-CastroDaniel Gallego-Perez

Sci. Adv., 7 (12), eabd4735. • DOI: 10.1126/sciadv.abd4735

Science Advances (ISSN 2375-2548) is published by the American Association for the Advancement of Science. 1200 New York Avenue NW, Washington, DC 20005. The title *Science Advances* is a registered trademark of AAAS.